

Strategies to Identify Boosted Tops

Jesse Thaler^{1,2}, Lian-Tao Wang³

¹ *Berkeley Center for Theoretical Physics, University of California, Berkeley, CA 94720*

² *Theoretical Physics Group, Lawrence Berkeley National Laboratory, Berkeley, CA 94720*

³ *Department of Physics, Princeton University, Princeton, NJ 08540*

Abstract

We study techniques for identifying highly boosted top jets, where the subsequent top decay products are not isolated. For hadronic boosted tops, we consider variables which probe the jet substructure in order to reduce the background from QCD jets with large invariant mass. Substructure variables related to two-body kinematics are least sensitive to the modeling of parton shower, while those which involve multi-body kinematics may still have discrimination power. For leptonic boosted tops, we consider variables which characterize the separation between the lepton—although not isolated by conventional criterion—and the hadronic activity in the top jet. Such variables are useful in reducing the backgrounds both from heavy-flavor jets and from accidental jet-lepton overlap. We give numerical estimates of the top identification efficiency versus background rejection rate as a functions of cuts on these variables, and find that these variables offer additional useful information above invariant mass alone.

Contents

1	Motivation	1
2	Top Decays vs. QCD Radiation	3
2.1	Jet Substructure Strategy	3
2.2	Choice of z Variable	5
2.3	Study of z Variable	7
3	Multi-Body Prospects	12
3.1	Theoretical Challenges	12
3.2	Boost-Invariant Event Shape	13
3.3	W Reconstruction	14
4	Leptonic Top Decays	16
4.1	Stuck Lepton Strategy	16
4.2	Lepton Variable Study	17
5	Conclusions and Outlook	22
A	The QCD Soft Singularity	23

1 Motivation

With over 10,000 top events at the Tevatron, CDF and D0 have begun to study the detailed properties and couplings of the top quark [1, 2]. At the upcoming Large Hadron Collider (LHC), the pair production cross section for top quarks approaches 1 nb [3], so with an estimated 100 million top events per year at peak luminosity, ATLAS and CMS will be able to pursue a program of precision top physics [4, 5].

Given the large top Yukawa coupling, it is natural to expect physics beyond the standard model (BSM) to have strong couplings to the top sector. Most solutions to the hierarchy problem require some kind of top partner [6, 7, 8, 9], and if that top partner is kinematically assessable at the LHC, then its decay products are expected to contain top quarks [10, 11, 12, 13]. Similarly, if the top quark is a semi-composite state [14], then new resonances in the composite sector are likely to have large branching fractions to top quarks [15].

At first glance, the near 100% branching ratio $t \rightarrow bW$ implies that any new physics that creates top quarks will be seen in events with multiple heavy-flavor-tagged jets and leptons. These exciting event topologies are somewhat challenging to reconstruct unambiguously, but in principle one can use standard methods [16, 4, 5] to identify top quarks coming from new physics. Indeed, tops produced nearly at rest in the lab frame have three isolated decay products which, apart from neutrinos and accidental overlap, can be separately identified. So assuming one can isolate a top-rich sample with well-identified decay products, the main challenge would be to separate a top-rich BSM signal from the SM top production background.

On the other hand, it is possible for a top-rich BSM signal to not have isolated decay products. If the top is produced with a considerable boost relative to the lab frame, then the three decay products from the top will end up in the same part of the detector and possibly be

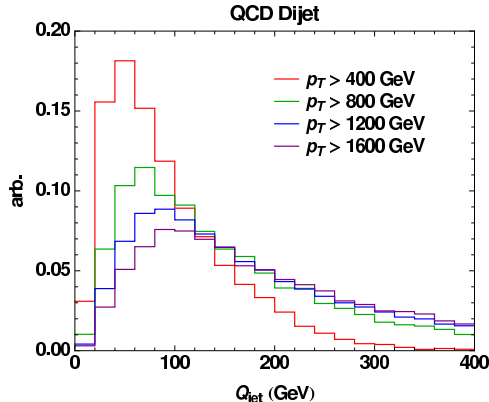


Figure 1: Distribution of the jet invariant mass of the hardest jet in QCD dijet production, for $p_T > 400, 800, 1200,$ and 1600 GeV. The average jet mass increases with jet p_T roughly as $10\% \times p_T$. In this and the remaining figures: the QCD production and showering are simulated using Pythia [17] (in this plot Pythia 8.108); FastJet 2.3.3 [18] is used for jet analysis; jets are identified using the anti- k_T algorithm [19] with $R_0 = 1.0$; the distributions are normalized to 1 to accentuate shape variations.

clustered into a single fat jet. This occurs for example with multi-TeV resonances that decay to tops [15], i.e. $X \rightarrow t\bar{t}$, where the boost factor $\gamma_t \sim m_X/(2m_t)$ can be large.

One background to these fat jets comes simply from high- p_T top events. Less obvious is that high- p_T QCD events also can yield fat jets. As shown in Fig. 1, the average invariant mass of a jet is around 10% ($\sim \alpha_s$) of its energy,¹ so once QCD jets have $p_T \sim 1$ TeV, the average jet invariant mass approaches the top mass. Said another way, the kinematics of top decays and the kinematics of QCD radiation start to look similar when $\gamma_t \sim 1/\alpha_s$. Depending on the performance of heavy-flavor tagging at high- p_T , one also worries about fat flavor-tagged jets, which could come from high- p_T bottom or charm production.

In this paper, we try to increase the purity for boosted top identification by finding variables that discriminate between boosted top jets and ordinary QCD fat jets. In Section 2, we consider boosted hadronic tops and study the energy asymmetry inside the jet. Because QCD splitting functions [20] have soft singularities, it is likely for a jet to have two subclusters with disparate energy scales. In contrast, an on-shell top decay yields a W and a b with roughly comparable energies. Energy asymmetry turns out to be the unique fat jet observable one can construct if one approximates the jet substructure by two-body kinematics, and it offers good separation between boosted tops from QCD fat jets. This variable is correlated with the d_{cut} measure used in preliminary boosted top studies at ATLAS [21]. In Section 3, we examine the prospects for identifying top jets through multi-body signatures. While the theoretical understanding of multi-body jet substructure is less controlled, we find that by identifying the hadronic W within a boosted top, one can obtain complementary information to energy asymmetry. Finally, in Section 4 we look at boosted leptonic tops and study the kinematics of the muon (or possibly electron) coming from the W decay. This muon is not isolated when the top is boosted, but the muon spectrum does discriminate between a boosted leptonic top, a bottom jet with a soft muon tag, and accidental jet-lepton overlap.

¹Depending on exactly what one means by “average invariant mass”, it may be more correct to say $m_{\text{jet}} \sim \sqrt{\alpha_s \log(E/E_0)}$, where E_0 is some reference energy.

The expected effectiveness of these variables depends crucially on the modeling the high p_T tail of the QCD background. In the context of a Monte Carlo simulation, to build up 170 GeV of radiation in a jet requires multiple QCD emissions. While the parton shower approximation is appropriate for describing emissions in the soft-collinear limit, the jet mass and the jet substructure depends crucially on how exactly the Monte Carlo program treats the kinematics of successive emissions. In this study, we focus on variables which are expected to be least sensitive to the details of the parton showering model, and we study model variance by using several showering algorithms. Ultimately, any fat jet variable will have to be tested on data and Monte Carlos tuned appropriately.

Our study focuses on the differences between QCD fat jets and boosted top jets without regard to any other features of the event. In most cases, the estimated top tagging efficiencies from this paper can be applied directly on top of a standard event selection criteria. However, this does mean that we will not discuss the absolute normalization of the background. One reason for this choice is that there are theoretical uncertainties in the size of the QCD jet invariant mass tail [22], so it is unknown precisely how much of the QCD dijet background enters the top mass window. Another reason is that depending on the specific BSM signal one is interested in, one would apply additional event selection criteria, and these criteria would dominantly affect the normalization of background and only secondarily the spectrum of the hardest fat jet. On the other hand, in many interesting new physics processes, boosted tops are pair produced, so there could be additional useful variables that correlate the two top quarks. Indeed, the QCD background to two fat jets will be different from the background to one fat jet. A full study of a boosted $t\bar{t}$ signal is beyond the scope of this paper and will be left to a future work.

2 Top Decays vs. QCD Radiation

2.1 Jet Substructure Strategy

When a boosted tops decays hadronically, there are no large sources of missing energy, so one can identify boosted top jets by finding jets with invariant mass $Q^2 \sim m_t^2$. Still, ordinary QCD jets can have large invariant mass, so one would like to extract some information about the substructure of the jet in order to better distinguish a top decay $t \rightarrow bW$ from a fat jet formed from QCD radiation.

In the parton shower approximation [23], the evolution of a QCD jet is described by a sequence of $1 \rightarrow 2$ splittings, such as the one shown in Fig. 2. After averaging over the azimuthal angle, there are only two variables that characterize the splitting $M \rightarrow AB$. One of them is the invariant mass (or virtuality) of the mother particle Q_M^2 . A typical and convenient choice for the other variable is the energy sharing

$$z_M = \frac{\min(E_A, E_B)}{E_M}. \quad (1)$$

All other choices for the two splitting variables are equivalent to $\{Q_M^2, z_M\}$ up to an ambiguity as to how to treat the invariant mass of the daughters A and B , which we discuss in more detail below. For the remainder of this section, we will only look at variables that can be characterized in terms of an $M \rightarrow AB$ splitting, leaving a discussion of the theoretical challenges and experimental prospects for multi-body signatures to Section 3.

Intuitively, differences between a QCD jet and a boosted top jet should only be significant during the early history of the shower, and the first splitting should be a “soft” splitting in the

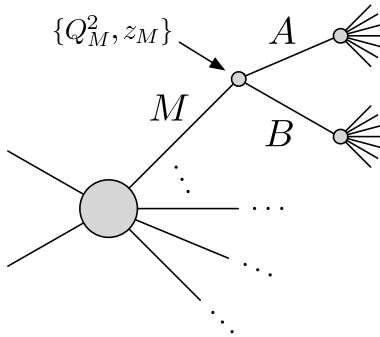


Figure 2: A schematic diagram of a $1 \rightarrow 2$ process as one stage of a parton shower history. For our study, the mother parton M is assumed to initiate a single jet, and the first splitting $M \rightarrow AB$ determines the dominant kinematic features of that jet. After integrating over azimuth, the first splitting it is determined by the jet invariant mass Q_M and the energy sharing $z_M = \min(E_A, E_B)/E_M$. Because of a theoretical ambiguity as to how to interpret the daughter invariant masses Q_A and Q_B , there are multiple z_M variants, each one giving a potential jet substructure observable.

case of QCD jet and a “hard” splitting in the case of the top jet. In Appendix A, we review two theoretical distributions for z_M . The narrow width approximation is a rough proxy for boosted tops, particularly for the first two stages of the prompt decay $t \rightarrow bW$ and $W \rightarrow q\bar{q}'$. The QCD parton shower gives a reasonable approximation to QCD fat jets, especially if we only look at the first splitting. In terms of $\{Q_M^2, z_M\}$, the differential decay distributions for the splitting $M \rightarrow AB$ take roughly the form

$$df_{M \rightarrow AB}^{\text{NWA}} \sim dQ_M^2 dz_M \delta(Q_M^2 - m_M^2), \quad m_M = m_t \text{ or } m_W \quad (2)$$

$$df_{M \rightarrow AB}^{\text{QCD}} \sim dQ_M^2 dz_M \frac{1}{Q_M^2} P(z_M), \quad (3)$$

where we have suppressed all non-singular functions. $P(z_M)$ is an Altarelli-Parisi splitting function [20] that typically scales like $1/z_M$.

Comparing df^{NWA} and df^{QCD} , the most obvious difference is the spectrum in Q_M , and as we already said, to distinguish a top jet from a QCD fat jet one first wants isolate a sample of jets with invariant mass close to m_t . But we see that the spectrum in energy sharing variable z_M is also different between top jets and QCD fat jets because of the soft singularity of QCD. In particular, df^{QCD} peaks towards $z_M \rightarrow 0$ in QCD, while df^{NWA} has its maximum at some finite value of z_M . If one can find an experimental observable that is correlated with z_M , then one would have an additional discriminating handle beyond just jet invariant mass.

In general, it will be difficult to find an experimental observable perfectly correlated with a parton shower history. In order to define the energy sharing z_M , one has to reconstruct the $M \rightarrow AB$ splitting, but we of course do not actually observe the showering process. However, recursive jet clustering algorithms [24, 25, 26, 27, 28, 19] are designed such that the jet clustering procedure approximately reverses the shower history. Given a set of particles that forms a jet M , one can apply a clustering algorithm until there are exactly two subclusters A and B .² As

²It is not necessary to use the same algorithm to define A and B as one used to find M . In this paper, we will in fact use two different procedures, anti- k_T for jet finding and k_T for subcluster finding.

long as the clustering procedure captures the leading singularities of QCD,³ the subclusters A and B will be reasonable proxies for the partons that participated in the first QCD splitting, and one can define z_M accordingly.

Of course, even with a perfect clustering algorithm, the experimentally identified subclusters A and B will not have a one-to-one relation to the theoretical splitting $M \rightarrow AB$. As an extreme example, even if A and B can be separately isolated in the rest frame of M , if the boost axis of the system is aligned with the momentum axis of A and B , then A and B will be perfectly overlapping and no experimental observable can disentangle them. In addition, finite calorimetry means that the QCD soft singularity is in effect regulated, so the experimental z_M distribution will always vanish as $z_M \rightarrow 0$. The hope is that the experimental and theoretical definitions of $M \rightarrow AB$ will agree some fraction of the time, so any experimental proxy for any z_M -like variable will offer some degree of discrimination power between top jets and QCD fat jets.

Finally, a comment about the criteria we use for identifying jets. In Section 2.3, we will define jets using a jet radius R which is larger than the values typically considered by ATLAS or CMS, and one might worry that we could obtain more information by using a stricter jet selection criteria. For finding boosted tops, though, choosing a smaller value of R only shifts the problem from tagging single jets with $Q \sim m_t$ to tagging pairs or trios of jets with $Q \sim m_t$. That is, even if on a lego plot it is “obvious” that a boosted top is composed of three objects, QCD fragmentation also has a finite probability of yielding three objects with $Q \sim m_t$. Whether one talks about jet substructure on a fat jet or interjet kinematics among smaller jets, one is faced with the same problem of trying to determine the identity of a set of objects with $Q \sim m_t$. That said, the value of R can certainly be optimized.

2.2 Choice of z Variable

The ideal choice for the z variable is one that is completely uncorrelated with jet invariant mass for QCD jets. In that case, one could imagine doing a sideband analysis to determine the expected QCD z distribution away from $Q^2 \sim m_t^2$ and then extrapolating to the top jet region. In Appendix A, we argue that in the leading logarithmic approximation, the variable that is most uncorrelated with invariant mass is the z_M variable that appears in the splitting function $P(z_M)$. That is, up to subleading corrections, the precise functional form of df^{QCD} in Eq. (26) can be written as the product of a Q_M^2 -dependent piece and a z_M -dependent piece.

This pseudo-factorization still does not tell us which definition of z_M to use. In order for the Alterelli-Parisi splitting function $P(z_M)$ to make sense, all that is required is that $z_M \rightarrow \min(E_A, E_B)/E_M$ in the limit that M , A , and B are exactly collinear and all on-shell. Given subcluster four vectors p_A and p_B , there are many functions $z_M(p_A, p_B)$ that satisfy this property, and they differ only by how the virtualities Q_A^2 and Q_B^2 of the daughters are treated.

In the context of a Monte Carlo simulation, each function $z_M(p_A, p_B)$ corresponds to different assumptions in the parton shower for how to treat successive emissions. This is referred to as momentum reshuffling [23] and occurs because the splitting $M \rightarrow AB$ with on-shell partons A and B has to be modified when A and B themselves split and go off-shell. The ideal choice for z is one that is uncorrelated with Q_M^2 *after* taking into account the spectra in Q_A^2 and Q_B^2 from subsequent splittings, but unfortunately, the information on the correct interpretation of

³In order to define z_M , it is important that the clustering scheme is “soft-sensitive”. For example, the recently proposed anti- k_T algorithm [19] performs clustering in a way that washes out information about the soft-singularity. Similarly, the distance measure used in the Cambridge/Aachen algorithm [28] also does not capture the soft singularity of QCD.

Q_A^2 and Q_B^2 is not contained in Eq. (26) and requires further insight from QCD. We discuss this issue more in Appendix A.

Given this ambiguity for how to define z , we present three plausible choices. The simplest experimental observable correlated with z is

$$z_{\text{cell}} = \frac{\min(E_A, E_B)}{E_A + E_B}, \quad E_X \equiv \sum_{i \in X} E_i, \quad (4)$$

where E_i are the energies of the calorimeter cells and the subclusters A and B are determined using some clustering scheme. This definition of z trivially satisfies the property that it asymptotes to $\min(E_A, E_B)/E_M$ in the exact collinear limit, though of course in the exact collinear limit, it is impossible to experimentally separate a jet into subclusters A and B .⁴

While simple, the above definition of z is by no means unique. A more complicated choice for a variable correlated with z is the d_{cut} variable used in the k_T jet clustering algorithm [27]. It has been used in the study of highly boosted W and Higgs jets [29] as well as for boosted tops [21]. In terms of the splitting $M \rightarrow AB$, d_{cut} is equivalent to

$$d_{\text{cut}} = \min(p_{TA}^2, p_{TB}^2) \Delta R_{AB}^2, \quad \Delta R_{AB}^2 \equiv (\phi_A - \phi_B)^2 + (\eta_A - \eta_B)^2, \quad (5)$$

where p_{Ti} , ϕ_i , and η_i , are the transverse momenta, azimuth, and pseudo-rapidity of A and B in the lab frame. The combination

$$z_{\text{cut}} \equiv \frac{d_{\text{cut}}}{d_{\text{cut}} + Q_M^2} \rightarrow \frac{\min(E_A, E_B)}{E_A + E_B} \quad (6)$$

in the limit that A and B are collinear and massless, so z_{cut} is a valid z -like variable.

One nice theoretical property of using z_{cut} as a discriminating variable compared to d_{cut} directly, is that d_{cut} measures both the soft ($z \rightarrow 0$) and collinear ($Q^2 \rightarrow 0$) singularities of QCD, whereas z_{cut} only captures the soft singularity. Therefore, we expect the z_{cut} -dependence to pseudo-factorize from the Q^2 -dependence, while d_{cut} is expected to be more correlated with Q^2 . Of course, once one isolates a sample of jets whose invariant mass is near a fixed value m_t , z_{cut} and d_{cut} perform nearly identically as discriminating variables for boosted tops. Experimentally, the reason to choose z_{cut} over d_{cut} would be if it is indeed more orthogonal to Q^2 , both in spectrum and in systematics.

There are Lorentz-invariant z variables such as

$$z_{\text{LI}} = \frac{\min(p_{\text{ref}} \cdot p_A, p_{\text{ref}} \cdot p_B)}{p_{\text{ref}} \cdot (p_A + p_B)}, \quad (7)$$

where p_{ref} is any reference four vector. It is easy to check that when p_A and p_B are massless and collinear, this yields a valid z -like variable as long as $p_{\text{ref}} \cdot (p_A + p_B)$ is not exactly zero. An obvious choice for p_{ref} is $p_A + p_B$ itself, but a downside to that choice is then z_{LI} can only go to zero when m_A or m_B goes to zero, so for typical fat QCD jets with many hadrons, z_{LI} never sees the QCD soft singularity. In the next section, we will take p_{ref} to be one of the proton beams $\{7 \text{ TeV}, 0, 0, 7 \text{ TeV}\}$,⁵ though this choice is not particularly well-motivated since

⁴The tension between a theoretical z that has to asymptote to a given value in the soft-collinear limit and an experimental z that has to know about the A/B distinction means that z cannot be defined using strictly collinear-safe observables. Said another way, to calculate the QCD z spectrum in perturbative theory, one would need to consider *two* partons per fat jet.

⁵Of course, the choice of the magnitude of p_{ref} does not affect our results.

it violates the reflection symmetry of the experiment. Note that z_{cell} is equivalent to choosing $p_{\text{ref}} = \{14 \text{ TeV}, 0, 0, 0\}$.

We emphasize that in the context of Eq. (3), z_{cell} , z_{cut} , z_{LI} , and all other z -like variables are completely equivalent. Because there is no preferred treatment of the virtualities Q_A^2 and Q_B^2 at the leading logarithmic level, we cannot say whether z should be a Lorentz-invariant function, or just a function of energy, or just a function of three-vectors. We also emphasize that one cannot decide which is the best definition of z from a showering Monte Carlo alone, because one would be sensitive to the momentum reshuffling assumptions of the algorithm.

2.3 Study of z Variable

We now study the z variables discussed in the previous section. Hard scattering, resonance decay, parton showering, and hadronization are performed with various versions of `Pythia` [17].⁶ We have used the `FastJet 2.3.3` [18] package to cluster and analyze the jets. No smearing of the jet or lepton energies have been included in this study. Because we will be using a clustering scheme to define observables, we have approximated the effect of detector resolution by including finite calorimeter segmentation. Hadrons are binned into $\delta\phi \times \delta\eta = 0.1 \times 0.1$ segments, and each segment is treated as a massless four-vector whose energy is determined by the hadronic energy deposit. The calorimeter extends to $|\eta| < 3.0$, and no charged track information is used. We will focus on the difference in the shapes of various observables, therefore all of the kinematical distributions from different processes are normalized to 1.

In all the analysis, we only use information about the hardest jet, and to find that jet we use the anti- k_T algorithm [19], which gives nearly conical jets, with $R_0 = 1.0$. As mentioned already, this value of R_0 is larger than the typical choices of 0.7 or 0.5, but is justified for the purposes of studying fat jets. In a more sophisticated analysis, one would choose different values of R_0 depending on the expected p_T spectrum of the boosted top in order to track the degree of collimation of the fat jet. In order to define the z variable, we have to identify the subclusters A and B . Taking only the calorimeter cells that formed the hardest jet, we recluster with the exclusive k_T algorithm [27] to force the formation of exactly 2 jets. This defines the full splitting $M \rightarrow AB$ from which we can define any z -like variable. Note that the jet finding algorithm is not the same as the jet substructure algorithm.

The source of highly boosted top jets in our study is a heavy resonance with a open decay mode $X \rightarrow t\bar{t}$. Because we only care about the z variable shape within a single jet, the total cross section and angular correlations for X production is irrelevant, though for definiteness we use a spin-1 sequential Z' [30], which is a `Pythia 8.108` default. The main effect of this choice is to select the PDFs used for production, which affects the η distribution of the boosted tops. We use three benchmark X masses, and corresponding cuts on the hardest jet p_T :

Resonance Mass	p_T Cut
2 TeV	800 GeV
3 TeV	1200 GeV
4 TeV	1600 GeV

(8)

For the QCD dijet background, we use three different versions of `Pythia` to estimate typical

⁶For simplicity, we have not considered underlying event or pile-up, though these effects are expected to degrade the performance of any jet-based measurement.

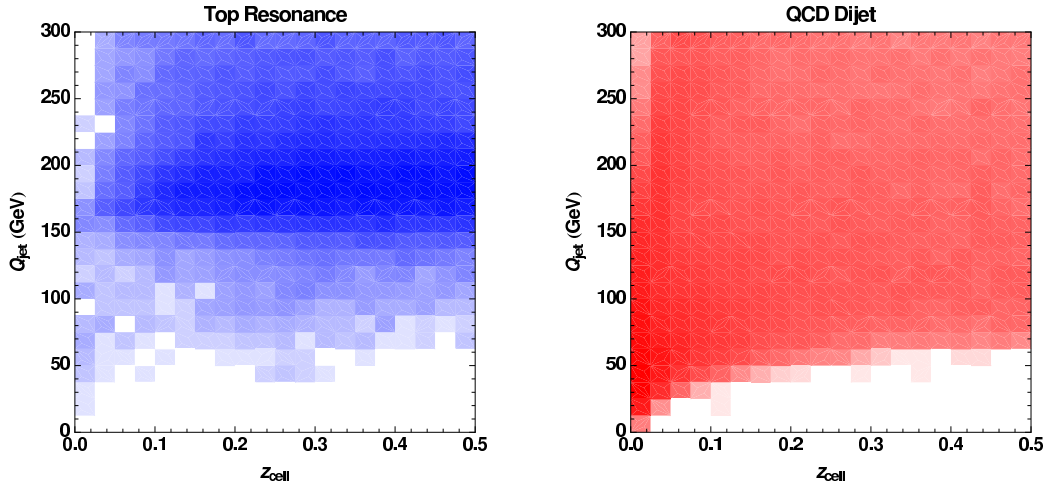


Figure 3: Two dimensional distributions of z_{cell} (horizontal axis) versus jet mass Q_{jet} (vertical axis) for the hardest jet with a 1200 GeV p_T cut. Left: boosted top jets from a 3 TeV resonance. The top quark resonance structure is visible as a dense horizontal band around $Q_{\text{jet}} \sim m_t$. Right: QCD dijet production. The infrared singularity is visible as $z \rightarrow 0$, though this feature is somewhat washed out at large Q_{jet} . The intensity of the shading is proportional to the logarithm of the occupancy.

variations among parton shower algorithms:

Name	Description
Pythia 8 (p_T)	Pythia 8.108 with the default p_T -ordered shower
Pythia 6 (p_T)	Pythia 6.409 with the “new” p_T -ordered shower (PYEVNW)
Pythia 6 (Q)	Pythia 6.409 with the “old” Q -ordered shower (PYEVNT)

(9)

We only consider light quark (uds) and gluon dijet production, though the inclusion of heavy-flavor (cb) does not dramatically change the distributions. Though SM $t\bar{t}$ production is an important background to $X \rightarrow t\bar{t}$, we consider high- p_T tops to be part of the signal for this study, and therefore do not include its contribution since the ratio between SM $t\bar{t}$ and BSM $t\bar{t}$ production is unknown. Because we are looking only at the hardest jet for analysis, the QCD background considered here is a reasonable proxy for any background with the jet p_T cut from Eq. (8).

In Fig. 3, we show two-dimension distributions for $\{Q_{\text{jet}}, z_{\text{cell}}\}$ for the 3 TeV top resonance and QCD dijets, both with a 1200 GeV p_T cut on the hardest jet. The top resonance near 170 GeV is visible in the signal sample, and the collinear and soft singularity near $Q^2, z \rightarrow 0$ is visible in the QCD sample. If the clustering procedure were to correctly identify the $t \rightarrow bW$ decay, then the expected z distribution from Eq. (2) would be nearly flat for the boosted top sample. Instead, we see that finite detector size and decay product overlap yields a z_{cell} distribution which falls off approximately linearly towards $z_{\text{cell}} \rightarrow 0$. In the QCD sample, the predicted $1/z$ behavior from Eq. (3) folded with the linear z_{cell} suppression flattens the z_{cell} distribution near $Q_{\text{jet}} = 170$ GeV, though the QCD soft singularity is still observable.

To isolate a boosted top sample, we first want to impose a jet invariant mass cut around top mass window $Q_{\text{min}} < Q_{\text{jet}} < Q_{\text{max}}$. Because we are using a largish value of R_0 , the top decay products are almost always clustered into a single jet, and choosing a fixed lower bound

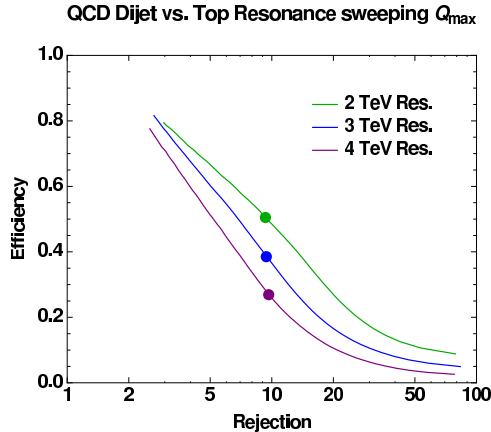


Figure 4: Signal efficiency versus background rejection using a top mass window selection criteria $160 \text{ GeV} < Q_{\text{jet}} < Q_{\text{max}}$ with varying Q_{max} . The background is QCD dijets from `Pythia 8.108`, and the signals and jet p_T cuts are given in Eq. (8). In this and the remaining efficiency vs. rejection plots, rejection r is defined as the fraction $1/r$ of the background remaining after the cut. The dots indicate the fiducial value $Q_{\text{max}} = 200 \text{ GeV}$.

of $Q_{\text{min}} = 160 \text{ GeV}$ only eliminates around 20% of the signal. The consequence of using such a large jet area is that additional hadronic activity from initial state radiation can enter the jet, so the signal has a long tail to larger values of Q_{jet} . In Fig. 4, we vary the value of Q_{max} and plot the rejection of the QCD background relative to the signal efficiency. For comparison with subsequent studies where we include additional variables, we choose a fiducial value of $Q_{\text{max}} = 200 \text{ GeV}$, labelled by the dots in Fig. 4. Amusingly, this value of Q_{max} gives the same 90% background rejection for all three benchmark p_T cuts, which can be understood from Fig. 1 because the normalized Q_{jet} distributions intersect near 170 GeV. As the resonance mass increases, the signal efficiency decreases, which is expected because contamination from initial state radiation is a bigger effect at larger parton collision energy, pushing the invariant mass of the top jet out of the top mass window. We expect that in a realistic study, one would optimize Q_{min} and Q_{max} in conjunction with R_0 .

Having identified the top mass window $160 \text{ GeV} < Q_{\text{jet}} < 200 \text{ GeV}$, we can use the z -variables to further purify the sample. We demonstrate typical z variable distributions in Fig. 5, again for the 3 TeV resonance benchmark. The jet invariant mass is shown in the upper left panel, and while one might be able to improve signal to background by tightening the top window criteria, invariant mass alone probably will not be completely effective in discriminating boosted top jets from QCD jets. The z -like variables discussed in the previous section, z_{cell} , z_{cut} and z_{LI} , all show a shape difference between boosted tops and QCD jets, with the QCD soft singularity clearly active. In Fig. 6, we assess the additional discrimination power offered by the z variable, and for a modest decrease in signal efficiency, one can increase the background rejection by a factor of 2 to 5 compared to an invariant mass cut alone. Instead of fixing the mass window, it is possible to achieve better results by optimizing Q_{max} and z_{cell} together. For example, from the right panel of Fig. 4, we see that in the case of 4 TeV resonance, the point with fiducial value $Q_{\text{max}} = 200 \text{ GeV}$ is somewhat below the curve from combined optimization. This is fairly common in other cases where we combine several variables.

The estimate of the QCD background shape depends on the modeling of the parton shower

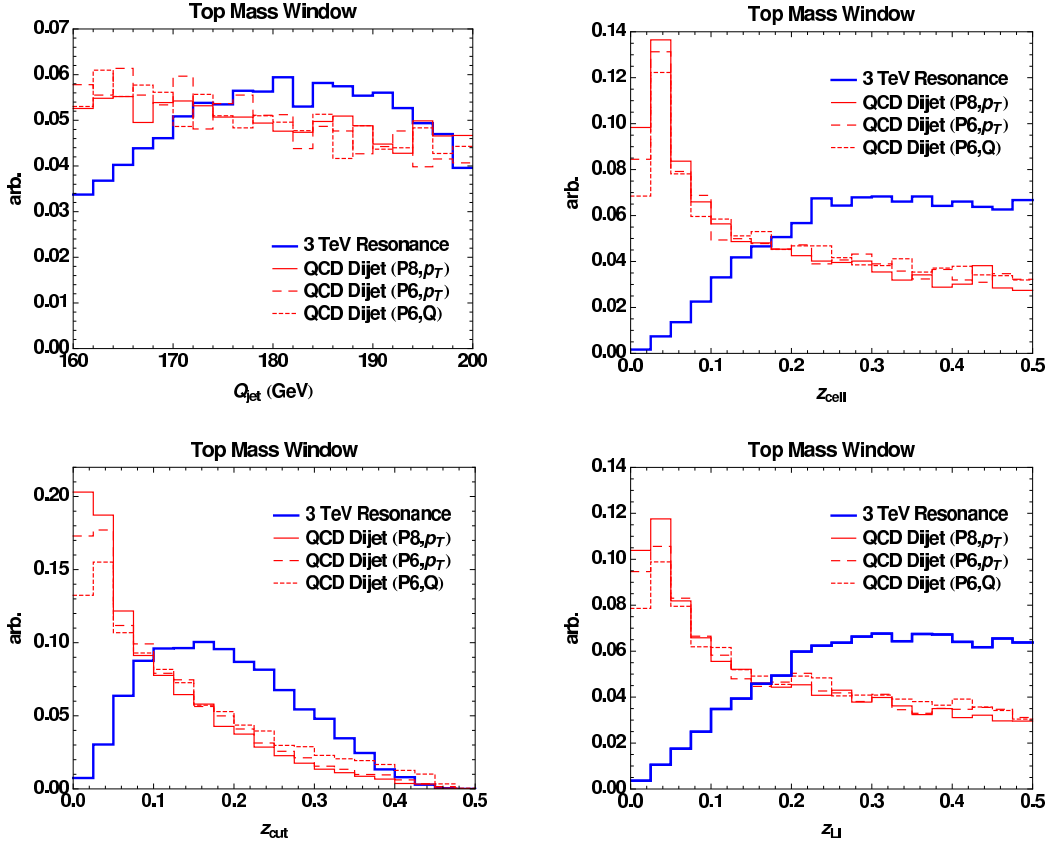


Figure 5: Fat jet spectra of the hardest jet after applying a top mass window $160 \text{ GeV} < Q_{\text{jet}} < 200 \text{ GeV}$ cut, comparing a 3 TeV top resonance with the QCD dijet background, both with a 1200 GeV p_T cut. From left to right, top to bottom: jet mass Q_{jet} , z_{cell} , z_{cut} , and z_{LI} . All three Pythia versions give similar spectra, validating our assumption that z variables should be relatively insensitive to showering assumptions. The dijet background peaks at $z = 0$, while the boosted top signal falls off linearly with z , so a z cut will provide additional discrimination power beyond jet mass alone.

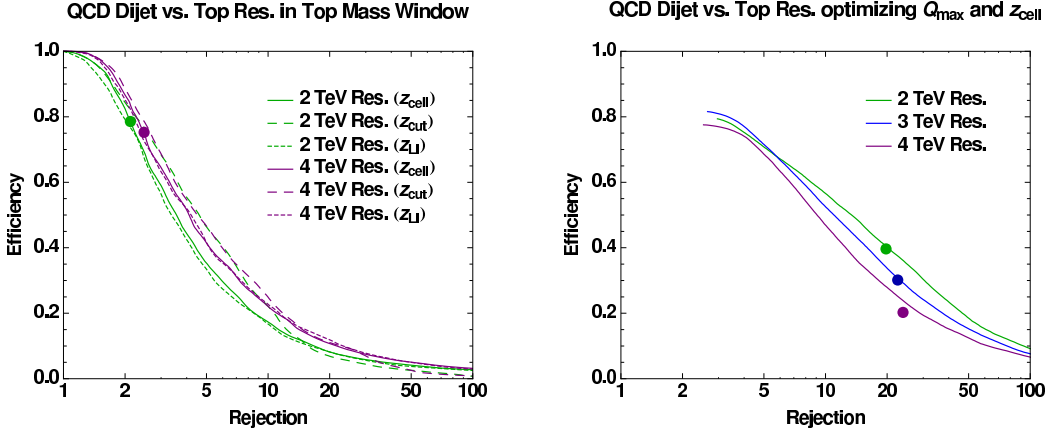


Figure 6: Signal efficiency versus background rejection using various z variables. Left: efficiency vs. rejection relative to the $160 \text{ GeV} < Q_{\text{jet}} < 200 \text{ GeV}$ top window cut. The dots indicate the fiducial value $\{Q_{\text{max}}, z_{\text{cell}}\} = \{200 \text{ GeV}, 0.2\}$. Right: optimizing the Q_{max} and z_{cell} cuts. This plot is directly comparable to Fig. 4.

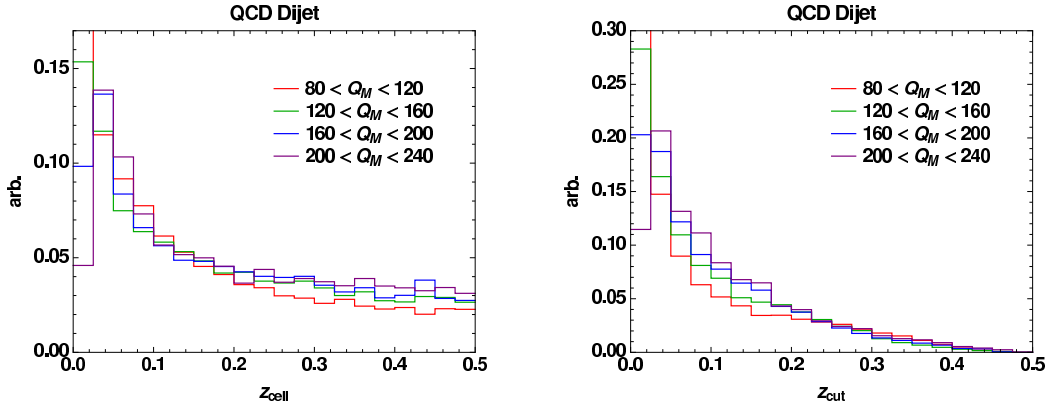


Figure 7: Evaluating the potential for a sideband study of z variables on QCD dijet production. While the strength of the soft singularity of QCD changes with different jet invariant mass cuts, the variation is modest, suggesting that the z spectrum can be measured at lower Q_{jet} and extrapolated to the top mass window. Left to right: z_{cell} and z_{cut} .

process, so it is encouraging that in Fig. 5, the three different showering algorithms give roughly the same z distributions. This suggests that the structure of the soft singularity is relatively insensitive to the showering assumptions, though this insensitivity is somewhat artificial since all three versions of `Pythia` use similar momentum reshuffling procedures, and therefore have the same preferred notion of z . In `Pythia 6 (Q)`, one can change the interpretation of z in the shower using the `MSTP(43)` option, but we found that these variations were no larger than the variations between different `Pythia` versions.

A realistic evaluation and optimization of the z -variable should be performed once we can study real QCD jets at the LHC. It is important to be able to perform such a study in a “side-band”, i.e. in a kinematical regime where the presence of top jets does not distort the infrared structure of QCD jets.⁷ In Fig. 7, we show the z -variable distribution for QCD jets for different jet mass windows. The variation in the z -distributions are mild across a wide range of jet masses, with the biggest difference being the peak shape near $z \rightarrow 0$, suggesting that a side-band study should be feasible.

3 Multi-Body Prospects

3.1 Theoretical Challenges

In the previous section, we looked at variables that approximated jet fragmentation as a simple two-body decay. Because we used a parton shower Monte Carlo to generate events, and because the parton shower is defined by a sequence of $1 \rightarrow 2$ splittings, we argued that the variables most likely to be correctly described by the Monte Carlo are ones that only involve a single $1 \rightarrow 2$ split. Given the momentum reshuffling ambiguity as to how to treat successive emissions in the parton shower, we wanted our analysis to be as independent of subsequent splittings as possible.

Because an $M \rightarrow AB$ splitting is characterized completely by Q_M^2 and z_M , many seemingly “better” observables are really equivalent to the analysis of Section 2 with a different choice of z variable. We already saw that there was a z_{cut} variable that captured the physics of a d_{cut} measurement. Similarly, an energy “dipole” variable is just a different way of phrasing $\{Q_M^2, z_M\}$. In principle, one could gain leverage by using information about the daughter virtualities, but already the different choices for z differ precisely by the treatment of Q_A^2 and Q_B^2 , so some of the daughter information is already contained in z . The only way to dramatically improve an analysis based on $M \rightarrow AB$ kinematics is to find experimental observables that do a better job correctly identifying the relevant subclusters A and B .

Given the limitations of two-body observables, one would like to look at multi-body signatures. Indeed, the decay of a top quark looks less like a $1 \rightarrow 2$ splitting and more like a $1 \rightarrow 3$ splitting, so one should be able to use multi-body information to help distinguish boosted tops from QCD jets. Such variables are not very well understood in the parton shower approximation, but in principle one could extend Eq. (3) to correctly handle multiple QCD emissions. Training such variables at the LHC with QCD jets in some proper control region will certainly provide useful information. With multi-body information about QCD, one can consider more elaborate jet substructure observables, and we will look at two specific kinds in this section.

⁷Away from $Q_{\text{jet}} \sim m_t$, there could be contamination from the signal if the top was far off-shell or if the supposed “top jet” only contained part of the top quark decay products. Because z distribution for a boosted top will be determined by a hard prompt decay, we expect the signal to be less sensitive to the theoretical uncertainties associated with parton shower modeling. Therefore any signal contamination effects could be estimated from Monte Carlo.

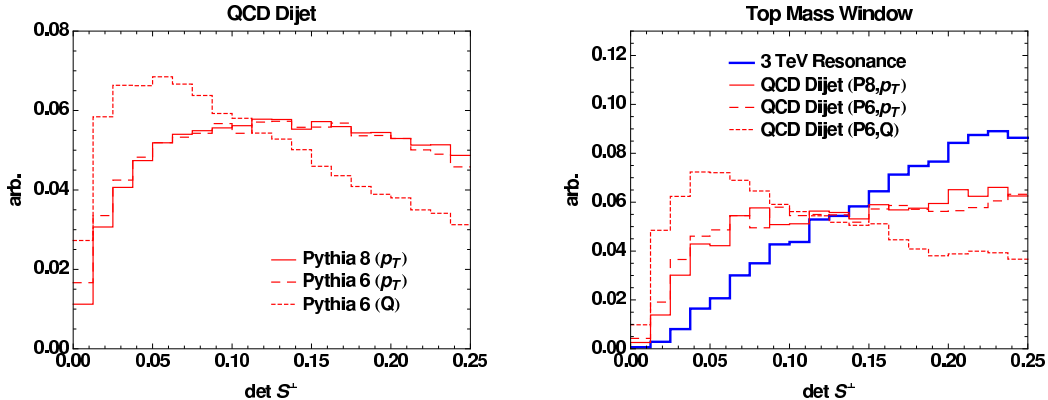


Figure 8: Left: QCD dijet predictions for $\det S^\perp$ with a p_T cut of 1200 GeV, showing large variations between different shower evolution variables. Right: $\det S^\perp$ after imposing the top window cut $160 \text{ GeV} < Q_{\text{jet}} < 200 \text{ GeV}$, comparing to a 3 TeV top resonance. While $\det S^\perp$ shows promise in separating boosted tops from QCD fat jets, it is difficult to make a firm conclusion given the large theoretical variance.

3.2 Boost-Invariant Event Shape

While boosted tops might be described theoretically by an $M \rightarrow ABC$ splitting, one still has to find an experimental proxy for the A , B , and C subclusters. Instead of using a clustering algorithm, an alternative strategy is to construct an event shape variable that uses all of the hadrons in a jet to form an observable that measures the gross energy distribution.

The goal is to build an event shape that probes the fact the top decay products are widely separated in the top rest frame, so one wants a boost-invariant event shape. Ideally, the event shape would be invariant under both the boost axis and the boost magnitude. Unfortunately, building a meaningful event shape that is invariant under choice of boost axis is difficult, because in the M rest frame, the splitting $M \rightarrow ABC$ defines a plane. If the boost axis is perpendicular to this plane then A , B , and C look well-separated, but if the boost axis is parallel to the plane, then A , B , and C overlap.

We can still form an event shape that is invariant under the boost magnitude, by considering a variant to the ordinary sphericity tensor [31].⁸ Taking the z -axis to be the boost direction, consider a jet with total four vector $\{E_{\text{jet}}, \vec{0}^\perp, p_{\text{jet}}^z\}$ and constituents $p_\alpha^\mu = \{E_\alpha, \vec{p}_\alpha^\perp, p_\alpha^z\}$. The (linear) jet transverse sphericity tensor $S^{\perp ij}$ is an object that is invariant under boosts along the z -axis:

$$S^{\perp ij} = \frac{\sum_{\alpha \in \text{jet}} \frac{\vec{p}_\alpha^{\perp i} \vec{p}_\alpha^{\perp j}}{|\vec{p}_\alpha^\perp|}}{\sum_{\alpha \in \text{jet}} |\vec{p}_\alpha^\perp|}. \quad (10)$$

There is only one non-trivial eigenvalue of S^\perp since the two eigenvalues sum to 1, so we will take the determinant of S^\perp to be our boost-invariant event shape. Note that $\det S^\perp$ is identically 0

⁸Strictly speaking, even this event shape is not invariant under boosts given finite calorimetry. Even though \vec{p}^\perp is invariant under boosts, the calorimetry is defined by ϕ and η , which is invariant only under boosts along the beam axis and not to boosts along the top momentum axis.

in the two-body limit, so $\det S^\perp$ does not have a z -like interpretation and is a true multi-body distribution. It is easy to check that $0 \leq \det S^\perp \leq 0.25$.

One can think of $\det S^\perp$ as measuring the degree of transverse phase space democracy within a jet. Boosted tops are peaked at large values of $\det S^\perp$ because when the boost axis is perpendicular to the ABC plane, the three decay products fill the transverse plane. QCD jets peak at smaller values of $\det S^\perp$ because filling the transverse plane would require two large kicks relative to the jet axis, but this is suppressed by the splitting functions.

While $\det S^\perp$ is a nice event shape in principle, it is not surprising that the theoretical distribution is not well understood in the parton shower picture. In the left panel of Fig. 8 we show the $\det S^\perp$ distribution for the three different versions of `Pythia` from Eq. (9), and one can see that depending on the choice of evolution variable in the shower, the prediction for the $\det S^\perp$ distribution can vary by 30%. In the right panel of Fig. 8, we isolate jets within the top mass window $160 \text{ GeV} < Q_{\text{jet}} < 200 \text{ GeV}$ and compare to a 3 TeV top resonance as in Section 2.3. Without information about which prediction is closer to true QCD, it is impossible to say how effective $\det S^\perp$ would be to separate signal from background.

3.3 W Reconstruction

The challenge to using event shapes is that they tend to probe the generic properties of jets and therefore require good theoretical control over QCD. A more promising approach is to look at observables that are very distinctive for boosted tops, such that one can be confident in their effectiveness even without accurate QCD predictions.

For boosted tops, the obvious distinguishing feature is the presence of an *on-shell* W inside a jet. Using a jet clustering algorithm to identify an $M \rightarrow ABC$ splitting, one can check whether a pair of A , B , and C reconstructs an 80 GeV resonance. In the left panel of Fig. 9, we use the same k_T clustering procedure as Section 2.3 to identify the $M \rightarrow ABC$ splitting, and plot the minimum pair-wise invariant mass Q_W between A , B , and C . One can see a clear peak at 80 GeV in the signal, and there is less variation in the different background estimates, though one should regard that observation with caution.

Once a candidate W is identified, one could try to use the same logic as Eqs. (2) and (3) to test for the QCD soft singularity with the supposed W jet. In the right panel of Fig. 9, we plot the z_W (defined analogously to z_{cell}) distribution for events with $60 \text{ GeV} < Q_W < 100 \text{ GeV}$. While there is a slight difference in shape, it is not nearly as dramatic as the shape variations seen in Fig. 5, probably because the overlap between subclusters is larger, blurring the QCD soft singularity.

Therefore, we conclude that the best use of hadronic W reconstruction is through a cut on Q_W . As seen in Fig. 10, Q_W seems to perform as well if not better than z_{cell} as a probe of boosted tops. Unfortunately, we have checked separately that Q_W and z_{cell} have correlated rejection rates, so one does not gain much by combining both cuts, though the systematics might be different enough to justify using both. In order to fully assess the effectiveness of W reconstruction against background, one should also study the background from boosted hadronic W s [29] with additional radiation, which will pass the Q_W cut more readily but fail the top window and z_{cell} criteria more often.

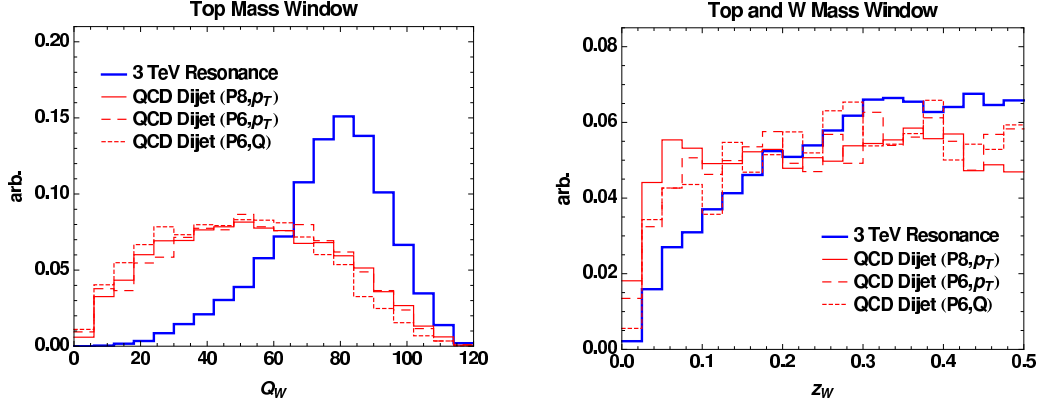


Figure 9: Left: applying the W reconstruction technique in the top mass window $160 \text{ GeV} < Q_{\text{jet}} < 200 \text{ GeV}$. A clear W resonance in Q_W is seen centered at 80 GeV for the top resonance, while QCD dijets are peaked at a lower value. Right: applying an additional W window cut $60 \text{ GeV} < Q_W < 100 \text{ GeV}$ and looking at z_W , the analog of z_{cell} within the candidate W . While there is some evidence of the QCD soft singularity as $z_W \rightarrow 0$, it is not strong enough to justify applying additional cuts on this variable.

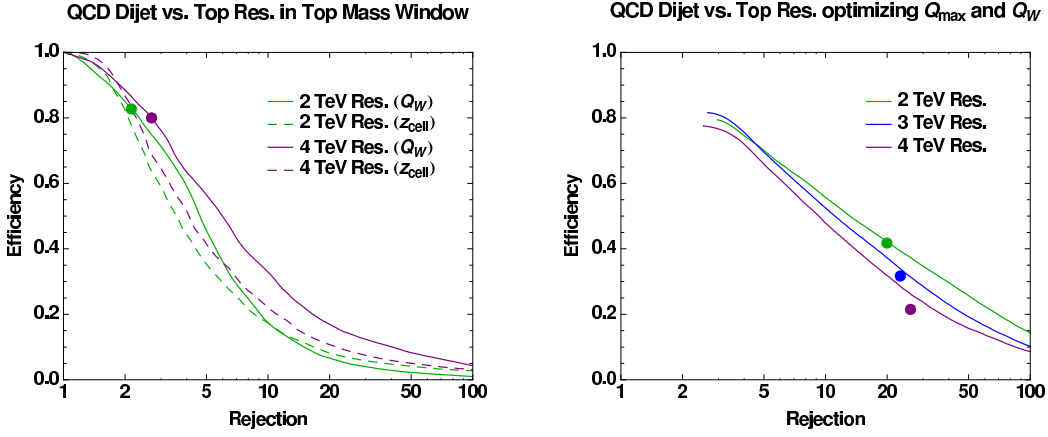


Figure 10: Signal efficiency versus background rejection using W reconstruction. Left: efficiency vs. rejection relative to the $160 \text{ GeV} < Q_{\text{jet}} < 200 \text{ GeV}$ top window cut. The z_{cell} distribution is shown for comparison, and the dots indicate the fiducial value $\{Q_{\text{max}}, Q_W\} = \{200 \text{ GeV}, 60 \text{ GeV}\}$. Right: optimizing the Q_{max} and Q_W cuts. This plot is directly comparable to Figs. 4 and 6.

4 Leptonic Top Decays

4.1 Stuck Lepton Strategy

When a top decays leptonically as $t \rightarrow b\ell\nu$, the neutrino carries away a substantial fraction of the top quark energy. It is straightforward to check that in this decay, the range achievable for $Q_{\text{visible}}^2 = (p_\ell + p_b)^2$ is

$$\frac{m_t^2 m_b^2}{m_t^2 - m_W^2} + \mathcal{O}(m_b^4) < Q_{\text{visible}}^2 < m_t^2 - m_W^2 + \mathcal{O}(m_b^2), \quad (11)$$

where we have taken the lepton to be massless for simplicity, and m_b should be regarded as the energy of the b jet including QCD radiation.⁹ Because this range extends down to very low values of Q_{visible}^2 , looking for jets with $Q^2 \sim m_t^2$ is no longer an efficient strategy for boosted top identification. Still, we will use Q_{visible}^2 as one selection criteria for boosted leptonic tops. We could in principle reconstruct the neutrino momentum and therefore the full kinematics in the semileptonic channel of QCD $t\bar{t}$ production, particularly near the threshold. However, depending on the particular top-rich BSM signal one is looking for, such reconstruction may not be feasible as there may be additional sources of missing energy in the event.

Even if one cannot use the invariant mass of visible objects to completely isolate boosted leptonic tops, the lepton from a boosted top is not isolated from the top jet hadronic activity, and the presence of a hard lepton “stuck” in a jet is still quite unique. One irreducible background comes from high- p_T bottom and charm jets as the decay of the resulting heavy flavor meson can contain leptons. Another irreducible background is $W/Z + \text{jets}$ where the gauge boson decays leptonically and the lepton “accidentally” gets caught in a jet. There is also a “background” to boosted leptonic tops from boosted hadronic tops with leptonic b decays, though the visible invariant mass can help separate these signals.

Because soft-muon tags are already used for b -tagging [4, 5], we will refer to the stuck lepton as a muon, though in principle, stuck electrons might also be observable.¹⁰ While our expectation is that muons should be relatively clean, potential fakes must be taken into account. Two common ways muon fakes can happen is kaon or pion decay in flight or if hadronic activity punches-through to the muon chamber [33]. In this work, we will not discuss these reducible backgrounds from lepton misidentification, though this might be more dangerous than the irreducible backgrounds because of the large rate for QCD jets. On the other hand, if the fake muon only carries a small fraction of the total hadronic energy, then the muon spectrum will be similar to heavy flavor jets, and we will see that we have good control over the heavy flavor background. For the numerical results presented in the rest of this section, we have not taken into account realistic lepton efficiencies and fake rates, and leave this to future study.

Unlike the case of hadronic tops, where there were large theoretical uncertainties in the jet substructure observables, we expect the leptonic variables to be well-modeled by (tuned) Monte Carlo. For the irreducible backgrounds, the source of the leptons are either W bosons or B mesons whose decays are well-understood. This leaves two main sources of theoretical uncertainty: the invariant mass spectrum of bottom and charm jets and the spectrum of the B and D meson inside the jet. The invariant mass spectrum should be measurable from data,

⁹In Eq. 11, we have not explicitly included possible missing energy in semileptonic B decays. This is expected to a subleading effect in evaluating Q_{visible}^2 . We do, however, take this effect into account in our numerical simulation.

¹⁰It is more challenging to identify an electron within a jet, although its different energy deposit pattern on the electromagnetic calorimeter combining with tracking information could be used [32].

using a sample of b -tagged but soft-muon-vetoed jets. One should also have some understanding of the B/D meson spectrum from the displaced vertex mass using the same sample.

4.2 Lepton Variable Study

To identify a candidate leptonic boosted top, we identify the muon with the hardest p_T in an event, and use the anti- k_T algorithm with $R_0 = 1.0$ to figure out which hadronic activity is associated with that muon. We call the muon four-vector p_μ and the remaining hadronic activity p_b , though we emphasize that we do not use b -tagging in this study and the hadronic activity need not initiated by heavy flavor such as the case of the $W/Z + \text{jets}$ background. We define three leptonic spectrum variables z_μ , ΔR , and x_μ and test their effectiveness for background rejection:

$$z_\mu = \frac{E_\mu}{E_\mu + E_b}, \quad \Delta R = \Delta R(p_\mu, p_b), \quad x_\mu = \frac{2p_\mu \cdot p_b}{(p_\mu + p_b)^2}. \quad (12)$$

We will describe the reason for these three variables in more detail below. In order to reject truly isolated muons, we impose a cut of $z_\mu < 0.9$ on all the samples. As in Section 2.3, we are focused on the shapes of the backgrounds, and normalize all distributions to 1.

For the boosted top signal, we will use the same X resonances as Section 2.3, with looser p_T requirements to account for the missing neutrino:

Resonance Mass	p_T Cut
2 TeV	600 GeV
3 TeV	800 GeV
4 TeV	1200 GeV

(13)

Using Monte Carlo truth information, we further divide the resonance signal into a leptonic sample where the muon comes from W decay and a hadronic sample where the muon comes from leptonic b decays. We use two different samples to estimate the irreducible backgrounds:

Name	Description
Heavy Flavor	Pythia 8.108 with $b\bar{b}$ and $c\bar{c}$ production
$W + \text{Jets}$	Pythia 8.108 with $W + j$ production, forcing $W \rightarrow \mu\bar{\nu}_\mu$

(14)

Because we only look at the hadronic activity surrounding the hardest muon, the $W + \text{jets}$ sample effectively includes the same physics as $Z + \text{jets}$. Similarly, the heavy flavor sample should give a reasonable approximation to any heavy flavor jet with the p_T cuts in Eq. (13).

In Fig. 11, we show two-dimension distributions for $\{Q_{\text{visible}}, x_\mu\}$ for the 3 TeV top resonance and the two background samples, all with an 800 GeV p_T (including the p_T of the muon) cut on the muonic jet. We plot x_μ only for comparison purposes, and will discuss the x_μ spectrum in more detail below. In order to isolate the boosted leptonic top sample, we want to impose a leptonic top mass window $Q_{\text{min}} < Q_{\text{visible}} < Q_{\text{max}}$. Since the heavy flavor dijet background is peaked at low values of Q_{visible} , we choose a reasonably hard cut of $Q_{\text{min}} = 100$ GeV. The effect of changing Q_{max} on efficiency versus rejection is shown in Fig. 12, and we take $Q_{\text{max}} = 200$ GeV as a fiducial value.

Leptonic spectra for the 3 TeV resonance after imposing the $100 \text{ GeV} < Q_{\text{visible}} < 200 \text{ GeV}$ leptonic top window are shown in Fig. 13. The simplest variable to understand is z_μ . A lepton from a top decay is prompt and therefore carries a large energy fraction of the top system. A lepton from a bottom (charm) jet comes only from the decay of a B (D) meson, but before the meson is formed, a significant fraction of the jet energy is already carried by radiated gluons.

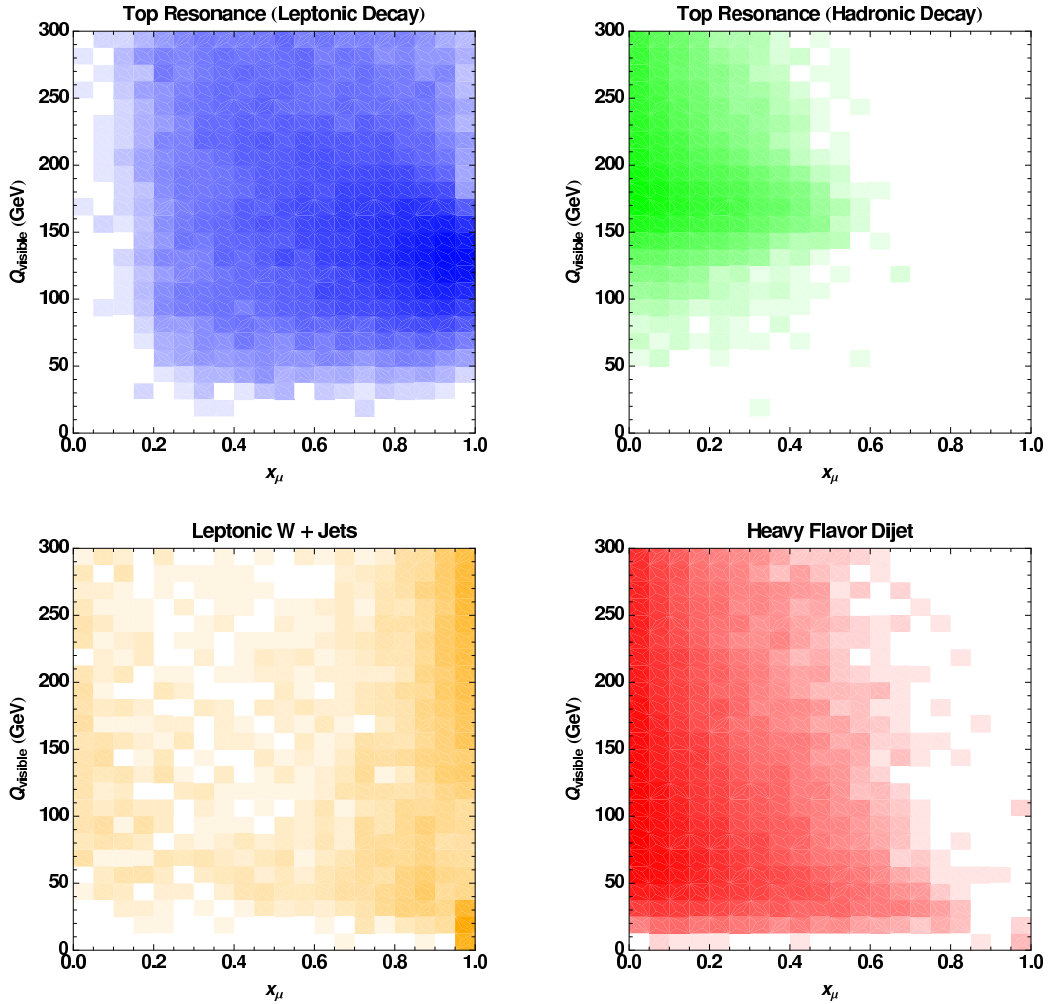


Figure 11: Two dimensional distributions of x_μ (horizontal axis) versus visible mass Q_{visible} (vertical axis) of the hardest muonic jet with a 800 GeV p_T cut (including p_T of muon). Top left: leptonic top decays. Because of the large neutrino missing energy, Q_{visible} peaks below m_t . As explained in the text, x_μ is peaked near 1 because most of the visible mass comes from the leptonic-hadronic angular separation. Top right: hadronic top decays with leptonic b decays. Since there is little missing energy in leptonic b decays, there is a peak at $Q_{\text{visible}} \sim m_t$. As explained in the text, x_μ peaks near 0 because most of the visible mass comes from hadronic system alone. Bottom left: W + jets production. Just like the leptonic top decay, x_μ is peaked near 1. Bottom right: Heavy flavor $b\bar{b}$ and $c\bar{c}$ production. Just like the hadronic top decay, x_μ is peaked near 0. The intensity of the shading is proportional to the logarithm of the occupancy.

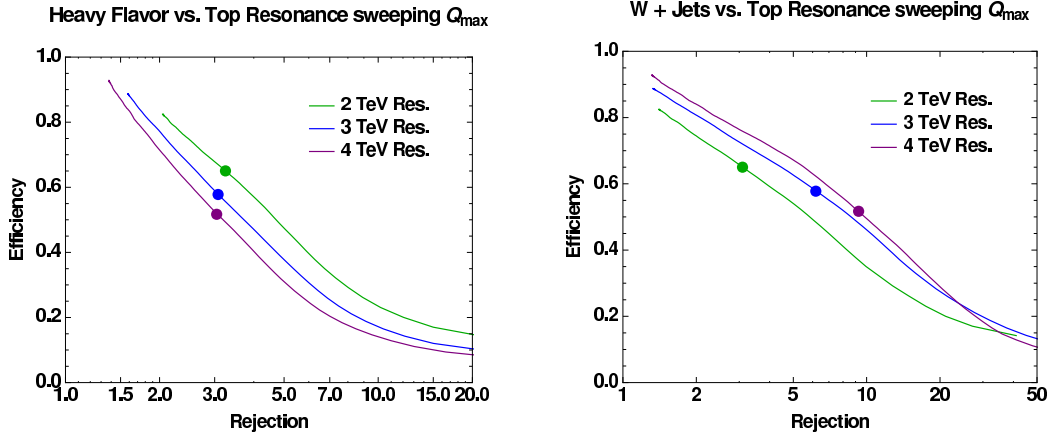


Figure 12: Signal efficiency versus background rejection using a leptonic top mass window selection criteria $100 \text{ GeV} < Q_{\text{visible}} < Q_{\text{max}}$ with a varying Q_{max} . The backgrounds and signals are described in Eqs. (13) and (14). Left: heavy flavor background. Right: W + jets background. The dots indicate the fiducial value $Q_{\text{max}} = 200 \text{ GeV}$. Because the leptonic top has a wider variation in visible mass than the hadronic case, invariant mass alone is not as efficient at rejecting background.

Therefore, z_{μ} is peaked closer to 0 both for heavy flavor jets and for hadronic tops with leptonic b decays. For the W + jets sample, z_{μ} peaks near 1 since most of the muons are isolated, but some fraction of the time a jet from initial state radiation can accidentally overlap with the muon.¹¹ The leptonic boosted tops occupies the middle range of z_{μ} and peaks at 0.4, consistent with the expectation that the muon should carry around 1/3 of the visible energy.¹²

The differences between the four samples are also seen in the angular separation ΔR between the muon and the hadronic activity. For heavy flavor jets, the muon is aligned almost exactly along the jet direction, as expected since the muon tracks the B meson which tracks the b quark. For hadronic tops with leptonic b decays, there is an additional deflection in ΔR from recoil against the W boson. The ΔR offset grows larger for leptonic tops since the bulk of the energy follows the hadronic activity. For W + jets the ΔR is random, as there is no intrinsic correlation between the muon direction and the hadronic activity.

Finally, a powerful variable for separating leptonic tops from heavy flavor jets is x_{μ} , which measures how much of the visible invariant mass is carried by the hadronic activity. Taking the muon to be massless, we can rewrite x_{μ} as

$$1 - x_{\mu} = \frac{m_b^2}{Q_{\text{visible}}^2}. \quad (15)$$

A boosted top has large p_T , but the invariant mass of the resulting b jet is expected to be around 10% of m_t since the available phase space is only a fraction of the top mass after sharing energy with the W boson, therefore x_{μ} is peaked towards 1. Similarly, W + jets peaks at $x_{\mu} = 1$ because the muon and the jet are uncorrelated and can be at large separation, meaning that $2p_{\mu} \cdot p_b$ tends to give the dominant contribution in $(p_{\mu} + p_b)^2$. For heavy flavor jets, the lepton carries

¹¹There is a small peak near $z_{\mu} = 0$ for the W + jets sample, because of $W + c$ production with leptonic D decays.

¹²A better estimate accounting for the W mass is $z_{\mu}^{\text{peak}} = (m_t^2 + m_W^2)/(3m_t^2 - m_W^2) \sim 0.44$.

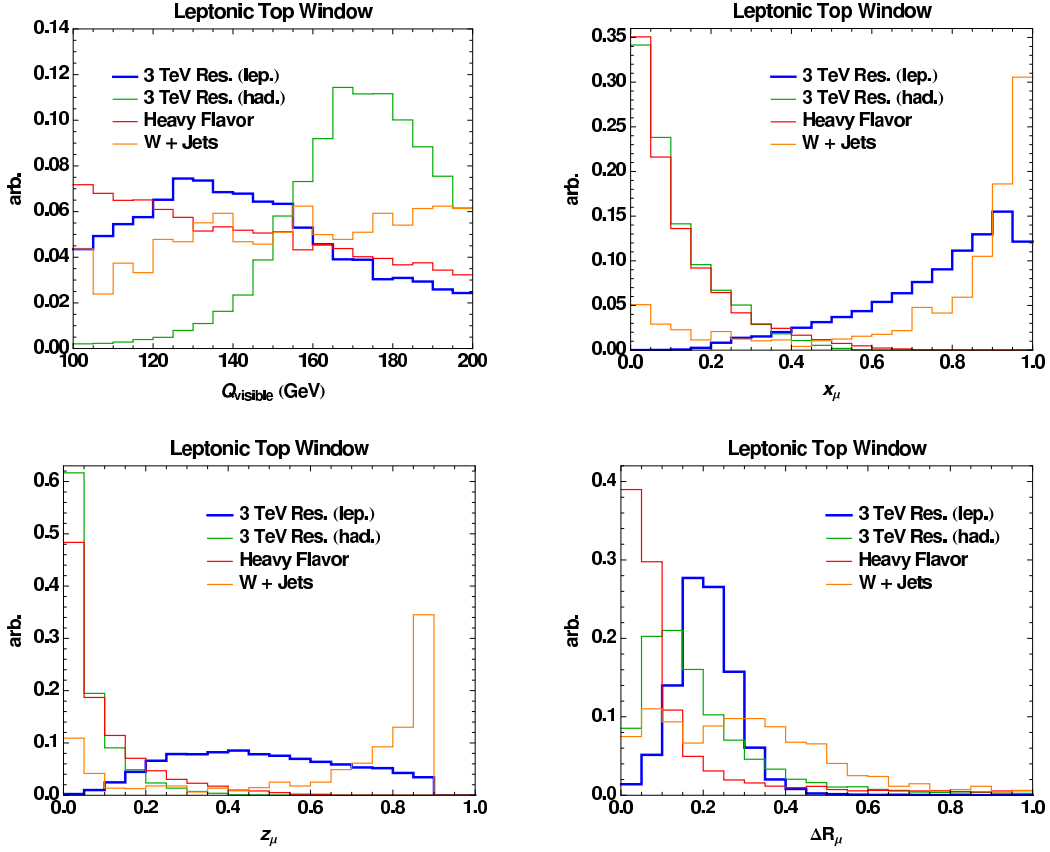


Figure 13: Muonic jet spectra of the hardest muonic jet after applying a leptonic top mass window $100 \text{ GeV} < Q_{\text{jet}} < 200 \text{ GeV}$ cut, comparing leptonic tops (blue) with hadronic tops with leptonic bs (green), the heavy flavor background (red), and the $W + \text{jets}$ background (orange). All samples have a jet p_T cut of 800 GeV. From left to right, top to bottom: visible mass Q_{visible} , x_{μ} , z_{μ} , and ΔR_{μ} . Descriptions of the behavior of these variables are given in the text.

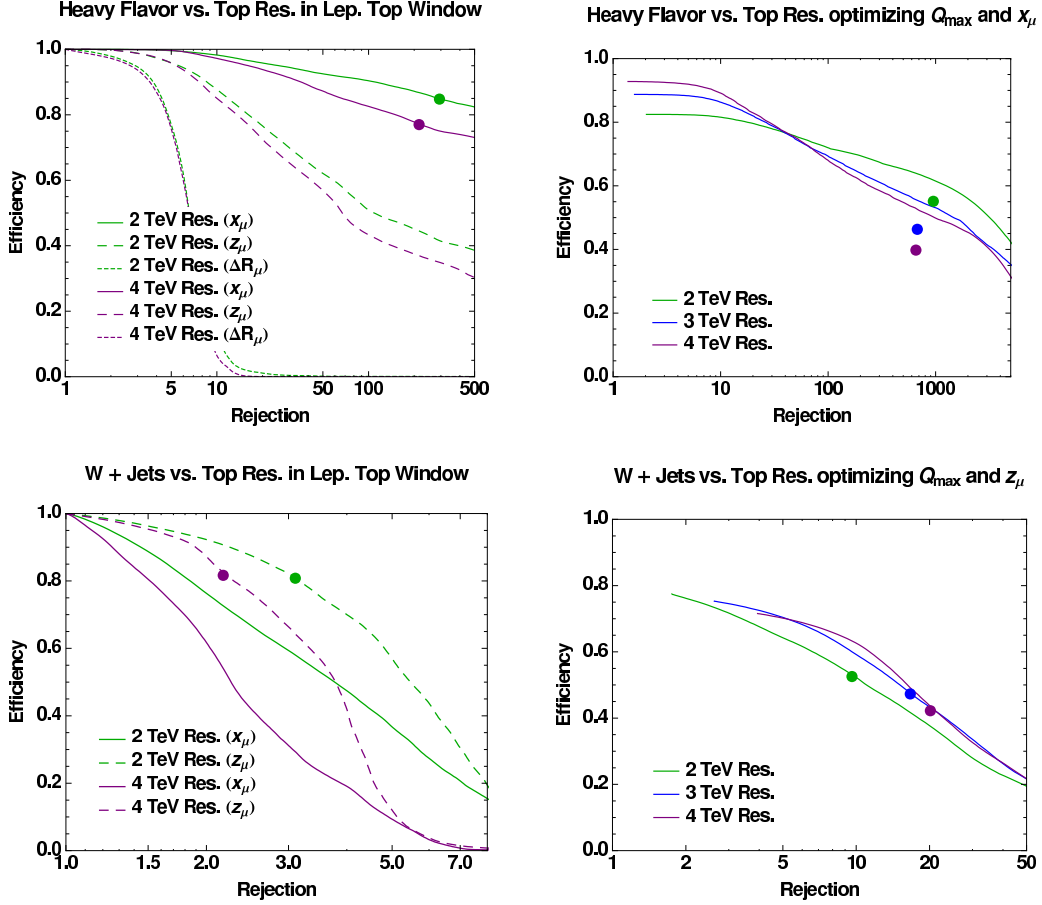


Figure 14: Signal efficiency versus background rejection using the various leptonic variables. The top row is the heavy flavor background and the bottom row is the $W + \text{jets}$ background. The left plots are efficiency vs. rejection relative to the $100 \text{ GeV} < Q_{\text{visible}} < 200 \text{ GeV}$ leptonic top window cut. The dots indicate the fiducial values $Q_{\max} = 200 \text{ GeV}$, $x_\mu = 0.6$, and $z_\mu = 0.7$. The plots in the right column are directly comparable to Fig. 12 and optimize Q_{\max} with respect to x_μ (for heavy flavor) or z_μ (for $W + \text{jets}$).

a small fraction of the energy, so in order for a heavy flavor jet to have large invariant mass, it must come mostly from the hadronic activity, yielding x_μ near zero. Hadronic tops are nearly identical to heavy flavor jets with the addition of extra hadronic activity from the W decay, so it also peaks at $x_\mu = 0$. Of course, to use x_μ effectively, one needs good momentum resolution on the muon, which becomes increasingly difficult at higher p_T .

In Fig. 14, we summarize the boosted leptonic top tagging efficiency versus background rejection using the three variables z_μ , ΔR , and x_μ . Without taking into account momentum resolution issues, it appears that the x_μ variable can be used to completely eliminate the heavy flavor background. Therefore, using a large x_μ cut along with b -tagging should give a very clean boosted leptonic top signal, because the b -tagging will help reduce the muon fake background. For rejecting the W + jets background, the z_μ variable gives a factor of 2 to 4 rejection for only a small loss in efficiency. It will be interesting to see how z_μ and x_μ perform to reduce the muon fake background in the absence of b -tagging. We also remark that the fraction of W + jets events in which the lepton actually overlaps with a jet is small since there is no obvious correlation between them.

5 Conclusions and Outlook

The top quark holds a unique position in both SM and BSM physics. As a SM resonance, it has a spectacular three-body decay with multiple distinguishing features like the b -tagged jet and the on-shell intermediate W boson. As a BSM focal point, it often has large couplings to new resonances and might be copiously produced in new physics signals. Depending on the mass scales involved, though, top quarks from BSM signals could be produced at large boosts, in which case the three-body nature of the top quark decay is obscured. While the large invariant mass of the top quark helps separate boosted tops from ordinary jets, fat jets are quite common at high p_T , therefore it is important to find complementary variables to help increase the purity of a boosted top signal.

For boosted hadronic tops, we found that jet substructure observables can give a factor of 2 to 5 better background rejection over invariant mass alone with only a moderate loss of signal efficiency. We classified jet substructure variables into those directly related to a $1 \rightarrow 2$ splitting process in the parton shower approximation and those involving multiple objects. Two-body observables are less sensitive to the parton shower modeling, and the energy sharing variable z provides additional information about the identity of a fat jet. There is in principle more information in multi-body signatures, and we found that W reconstruction was a promising strategy for boosted top identification, however more theoretical studies are needed to understand multi-body jet substructure.

For boosted leptonic tops, one can look for a hard muon surrounded by hadronic activity, and we found that the spectrum of the muon relative to the hadronic activity gave excellent rejection against the irreducible backgrounds. In particular, the heavy flavor background could be almost completely eliminated through the x_μ variable, and the W/Z + jets background could be made manageable through the z_μ variable. However, further study is needed to understand the issue of lepton fakes to test whether the spectrum of muons from inflight decay or punch-through is sufficiently different from boosted tops.

In this study, we suggested variables based only on theoretical considerations, and tested their effectiveness with minimal realism on calorimeter segmentation. In order to optimize these variables and obtain realistic estimates of tagging efficiencies versus background rejection, one needs to include more detector effects, such as tracking information, energy/momentum

resolution, and fakes. Full optimization of cuts should come after training these variables on real jets at the LHC. One important omission is that we did not make use of b -tagging, which should help improve rejection against QCD fat jets and lepton fakes, though the efficiency of b -tagging for boosted tops at high p_T is expected to decrease [34].

The results of this paper apply to the properties of individual fat jets, ignoring any other features of the event. In many BSM scenarios, the signal is found not just with a single boosted top but in a boosted $t\bar{t}$ channel. Therefore, in addition to the single top tagging observables we have studied in this paper, variables which correlate the two top jets should be explored to enhance the signal reach.

Acknowledgements

We would like to thank Ben Lillie and Lisa Randall for collaboration during the early stages of this project and for many valuable discussions on jet substructures. We would also like to thank Aaron Pierce and Jianmin Qian for discussions regarding leptonic variables. J.T. is supported by a fellowship from the Miller Institute for Basic Research in Science. The work of L.W. is supported by the National Science Foundation under Grant No. 0243680.

Shortly after this paper was posted, Ref. [36] appeared which presented a complementary boosted top strategy.

A The QCD Soft Singularity

In order to understand the QCD soft singularity, we have to understand the expected z distribution. For illustrative purposes, we will compare the z distribution between a narrow resonance decay and QCD radiation. Because the decay products of a boosted top are generically overlapping, we do not expect a boosted top to look exactly like the narrow width expectation, but such a comparison is still instructive. To begin, we will describe two-body phase space variables and then compare the differential distributions between the two cases.

Consider the process $pp \rightarrow XAB$, where A and B are subclusters of interest, and X is every other final state in the event. We want to approximate the cross section for this process in a factorized form as

$$d\sigma_{pp \rightarrow XAB} = d\sigma_{pp \rightarrow XM} df_{M \rightarrow AB}, \quad (16)$$

where the ‘‘mother’’ parton M is a proxy for the fat jet. If M is a resonance, then such a factorized form can be justified in the narrow width approximation, with $df_{M \rightarrow AB}$ being a differential branching ratio. This factorized form also makes sense in the soft-collinear limit, where $df_{M \rightarrow AB}$ is the product of a differential splitting function [20] and a Sudakov factor [35].

The phase space variables for the ‘‘decay’’ $M \rightarrow AB$ (with masses Q_M , Q_A , and Q_B , respectively) are

$$\frac{dQ_M^2}{2\pi} d\Phi_2^{M \rightarrow AB}, \quad (17)$$

where the on-shell two body phase space is given by

$$d\Phi_2^{M \rightarrow AB} = \frac{\lambda(Q_M^2; Q_A^2, Q_B^2)}{32\pi^2} d\Omega_2, \quad d\Omega_2 \equiv d\cos\theta d\phi, \quad (18)$$

with the usual phase space factor

$$\lambda(Q_M^2; Q_A^2, Q_B^2) = \sqrt{\left(1 - \frac{Q_A^2}{Q_M^2} - \frac{Q_B^2}{Q_M^2}\right)^2 - 4\frac{Q_A^2}{Q_M^2}\frac{Q_B^2}{Q_M^2}}. \quad (19)$$

For unpolarized measurements, the ϕ -dependence is uniform, so the phase space of $M \rightarrow AB$ is characterized by two independent quantities Q_M and $\cos\theta$. In order to study the QCD soft singularity, the natural variables for fat jets are the invariant mass Q_M and some energy sharing variable $z = E_A/E_M$,¹³ and in general there will be a Jacobian $d\cos\theta/dz$ in the transformation from $\cos\theta$ to z .

If z is interpreted strictly as E_A/E_M , then two-body kinematics restricts the range for z to be

$$\left| z - \frac{1}{2} \left(1 + \frac{Q_A^2}{Q_M^2} - \frac{Q_B^2}{Q_M^2} \right) \right| \leq \frac{\beta_M}{2} \lambda(Q_M^2, Q_A^2, Q_B^2), \quad \beta_M = \sqrt{1 - Q_M^2/E_M^2}, \quad (20)$$

where β_M is the boost magnitude from the M center-of-mass frame to the lab frame. Because these limits depend on Q_A and Q_B , in a parton shower with multiple emissions, the correct z limits on $M \rightarrow AB$ can only be determined after one knows how A and B will split which sets the values of Q_A and Q_B . In particular, a value of z that satisfies Eq. (20) for $Q_{A,B} = 0$ might be invalid for $Q_{A,B} > 0$. There are various ways to deal with this ambiguity [23], and most parton showers employ some kind of momentum reshuffling procedure, but it means that the interpretation of z in $df_{M \rightarrow AB}$ can depend on Q_A and Q_B in a non-trivial and algorithm-specific way.

We can now compare the differential distributions $df_{M \rightarrow AB}$ between the narrow width approximation and QCD radiation. In the narrow width approximation, the mother M is exactly on-shell:

$$df_{M \rightarrow AB}^{\text{NWA}} = \frac{dQ_M^2}{2\pi} \frac{d\Phi_2^{M \rightarrow AB}}{V_2} \text{Br}(M \rightarrow AB) \delta(Q_M^2 - m_M^2), \quad (21)$$

where $V_2 \equiv \int d\Phi_2$ is the volume of two-body Lorentz invariant phase space, which depends on the masses of A and B . Note that df^{NWA} is uniform in $\cos\theta$.

In the soft-collinear QCD case, one can use a parton shower language [23] where the natural variables are the evolution variable μ and the energy sharing variable z , both of which are functions of $\{Q_M^2, \cos\theta\}$. Unlike the narrow width approximation, the parton M is never on-shell, and its off-shellness is determined by the evolution variable $\mu(Q_M^2, \cos\theta)$. Using unpolarized splitting functions defined in terms of the energy sharing variable $z(Q_M^2, \cos\theta)$, the QCD splitting is described by

$$df_{M \rightarrow AB}^{\text{QCD}} = d \log \mu^2 \frac{d\phi}{2\pi} dz \frac{\alpha_s(\mu)}{2\pi} P_{M \rightarrow AB}(z) \Delta(\mu_{\text{start}}, \mu), \quad (22)$$

where $P_{M \rightarrow AB}(z)$ are the usual Altarelli-Parisi splitting functions [20]

$$\begin{aligned} P_{q \rightarrow qg}(z) &= C_F \frac{1+z^2}{1-z}, \\ P_{g \rightarrow gg}(z) &= C_A \left[\frac{1-z}{z} + \frac{z}{1-z} + z(1-z) \right], \\ P_{g \rightarrow q\bar{q}}(z) &= T_R [z^2 + (1-z)^2], \end{aligned} \quad (23)$$

and $\Delta(\mu_{\text{start}}, \mu)$ is a Sudakov factor [35]

$$\Delta(\mu_{\text{start}}, \mu) = \exp \left[- \sum_{AB} \int_{\mu}^{\mu_{\text{start}}} d \log \mu' \int \frac{d\phi}{2\pi} \int dz \frac{\alpha_s(\mu')}{2\pi} P_{M \rightarrow AB}(z) \right]. \quad (24)$$

¹³In the main body of the text, we define z as $\min(E_A, E_B)/E_M$ since A and B are indistinguishable. Here, A and B have meaningful quantum numbers, so it makes sense to talk about $z = E_A/E_M$.

Note the soft singularities at $z \rightarrow 0$ or $z \rightarrow 1$ which are equivalent to singularities at $|\cos \theta| \rightarrow 1$.

We want to describe both df^{NWA} and df^{QCD} in terms of the natural boosted top variables Q_M^2 and z . We have not yet specified the functional form of μ and z , and in general, there will be a non-trivial Jacobian in the transformation between $\{\mu, z\}$ and $\{Q^2, \cos \theta\}$. Typical evolution variables are proportional to invariant mass as $\mu^2 = Q_M^2 f(z)$, in which case $d \log \mu^2 = d \log Q_M^2$. Integrating over ϕ for simplicity

$$df_{M \rightarrow AB}^{\text{NWA}} = \frac{dQ_M^2}{2\pi} dz \frac{d \cos \theta}{dz} \text{Br}(M \rightarrow AB) \delta(Q_M^2 - m_M^2), \quad (25)$$

$$df_{M \rightarrow AB}^{\text{QCD}} = \frac{dQ_M^2}{2\pi} dz \frac{1}{Q_M^2} \frac{\alpha_s(\mu)}{(2\pi)} P_{M \rightarrow AB}(z) \Delta(\mu_{\text{start}}, \mu), \quad (26)$$

where μ is still a function of Q^2 and z . Assuming that $d \cos \theta / dz$ does not contain any singularities, this function has the form advertised in Eqs. (2) and (3). If $Q_A = Q_B = 0$, then $d \cos \theta / dz = 2/\beta_M$.

We see that df^{QCD} does not factorize into a Q_M^2 -dependent and a z -dependent piece, because the α_s factor and Sudakov factor are written in terms of the evolution variable μ that mixes Q^2 and z . On the other hand, at the double logarithmic level the value α_s is fixed, and because the definition of μ_{start} is ambiguous in the Sudakov factor, the value of μ_{start} can be chosen remove the z -dependence up to subleading corrections. In other words, the non-factorizing pieces occur only at the single logarithmic level, so df^{QCD} does factorize in the leading logarithmic approximation.

To design the perfect z -variable for boosted tops, one would want to figure out which z -like variable is maximally orthogonal to Q^2 for real QCD in the neighborhood of $Q^2 \sim m_t^2$. This requires understanding the spectrum of Q_A and Q_B from subsequent splittings and how they influence the interpretation of z . Whether this is in principle possible depends on whether the leading corrections to df^{QCD} still respect the factorized form of Eq. (16). If higher order QCD corrections simply modify the functional form of df^{QCD} , then there is always some variable z that is orthogonal to Q^2 , though in practice it may be difficult to find an experimental observable correlated with z . But if higher order QCD corrections imply that the ideal choice of z variable strongly depends on the spectators X in the process $pp \rightarrow XAB$, then there is no way to improve the definition of z . A plausible intermediate possibility is that df^{QCD} depends on X only in some limited way such as in the definition of μ_{start} . If z -like variables are found to be useful in an experimental context, then a detailed study of df^{QCD} is warranted.

References

- [1] <http://www-cdf.fnal.gov/physics/new/top/top.html>
- [2] <http://www-d0.fnal.gov/Run2Physics/WWW/results/top.htm>
- [3] R. Bonciani, S. Catani, M. L. Mangano and P. Nason, Nucl. Phys. B **529**, 424 (1998) [arXiv:hep-ph/9801375]. For recent updates, see S. Moch and P. Uwer, arXiv:0804.1476 [hep-ph]; M. Cacciari, S. Frixione, M. M. Mangano, P. Nason and G. Ridolfi, arXiv:0804.2800 [hep-ph]; N. Kidonakis and R. Vogt, arXiv:0805.3844 [hep-ph].
- [4] “ATLAS: Detector and physics performance technical design report. Volume 1,” CERN-LHCC-99-14.
“ATLAS detector and physics performance. Technical design report. Vol. 2,” CERN-LHCC-99-15

- [5] CMS Technical Design Report V.1., CERN-LHCC-2006-001, CMS Technical Design Report V.2., CERN-LHCC-2006-021
- [6] S. Dimopoulos and H. Georgi, Nucl. Phys. B **193**, 150 (1981).
- [7] T. Appelquist, H. C. Cheng and B. A. Dobrescu, Phys. Rev. D **64**, 035002 (2001) [arXiv:hep-ph/0012100].
- [8] N. Arkani-Hamed, A. G. Cohen and H. Georgi, Phys. Lett. B **513**, 232 (2001) [arXiv:hep-ph/0105239].
- [9] Z. Chacko, H. S. Goh and R. Harnik, Phys. Rev. Lett. **96**, 231802 (2006) [arXiv:hep-ph/0506256].
- [10] H. C. Cheng, I. Low and L. T. Wang, Phys. Rev. D **74**, 055001 (2006) [arXiv:hep-ph/0510225].
- [11] P. Meade and M. Reece, Phys. Rev. D **74**, 015010 (2006) [arXiv:hep-ph/0601124].
- [12] A. Freitas and D. Wyler, JHEP **0611**, 061 (2006) [arXiv:hep-ph/0609103]. A. Belyaev, C. R. Chen, K. Tobe and C. P. Yuan, arXiv:hep-ph/0609179.
- [13] S. Matsumoto, M. M. Nojiri and D. Nomura, Phys. Rev. D **75**, 055006 (2007) [arXiv:hep-ph/0612249]; M. M. Nojiri and M. Takeuchi, arXiv:0802.4142 [hep-ph].
- [14] T. Gherghetta and A. Pomarol, Nucl. Phys. B **586**, 141 (2000) [arXiv:hep-ph/0003129]. K. Agashe, A. Delgado, M. J. May and R. Sundrum, JHEP **0308**, 050 (2003) [arXiv:hep-ph/0308036].
- [15] K. Agashe, A. Belyaev, T. Krupovnickas, G. Perez and J. Virzi, Phys. Rev. D **77**, 015003 (2008) [arXiv:hep-ph/0612015]. V. Barger, T. Han and D. G. E. Walker, Phys. Rev. Lett. **100**, 031801 (2008) [arXiv:hep-ph/0612016]. B. Lillie, L. Randall and L. T. Wang, JHEP **0709**, 074 (2007) [arXiv:hep-ph/0701166]. A. L. Fitzpatrick, J. Kaplan, L. Randall and L. T. Wang, JHEP **0709**, 013 (2007) [arXiv:hep-ph/0701150]. K. Agashe, H. Davoudiasl, G. Perez and A. Soni, Phys. Rev. D **76**, 036006 (2007) [arXiv:hep-ph/0701186]. U. Baur and L. H. Orr, Phys. Rev. D **76**, 094012 (2007) [arXiv:0707.2066 [hep-ph]]. R. Frederix and F. Maltoni, arXiv:0712.2355 [hep-ph]. U. Baur and L. H. Orr, arXiv:0803.1160 [hep-ph].
- [16] B. Abbott *et al.* [D0 Collaboration], Phys. Rev. D **58**, 052001 (1998) [arXiv:hep-ex/9801025]. F. Abe *et al.* [CDF Collaboration], Phys. Rev. Lett. **80**, 2767 (1998) [arXiv:hep-ex/9801014].
- [17] T. Sjostrand, S. Mrenna and P. Skands, JHEP **0605**, 026 (2006) [arXiv:hep-ph/0603175]. T. Sjostrand, S. Mrenna and P. Skands, arXiv:0710.3820 [hep-ph].
- [18] M. Cacciari and G. P. Salam, Phys. Lett. B **641**, 57 (2006) [arXiv:hep-ph/0512210], <http://www.lpthe.jussieu.fr/~salam/fastjet/>.
- [19] M. Cacciari, G. P. Salam and G. Soyez, JHEP **0804**, 063 (2008) [arXiv:0802.1189 [hep-ph]].
- [20] G. Altarelli and G. Parisi, Nucl. Phys. B **126**, 298 (1977).
- [21] G. Brooijmans, ATLAS note, ATL-PHYS-CONF-2008-008.

- [22] L. Almeida, S. J. Lee, G. Perez, G. Sterman, I. Sung, J. S. Virzi, in preparation.
- [23] T. Sjostrand, P. Eden, C. Friberg, L. Lonnblad, G. Miu, S. Mrenna and E. Norrbin, *Comput. Phys. Commun.* **135**, 238 (2001) [arXiv:hep-ph/0010017]. T. Sjostrand and P. Z. Skands, *Eur. Phys. J. C* **39**, 129 (2005) [arXiv:hep-ph/0408302]. G. Corcella *et al.*, *JHEP* **0101**, 010 (2001) [arXiv:hep-ph/0011363]. R. Kuhn, F. Krauss, B. Ivanyi and G. Soff, *Comput. Phys. Commun.* **134**, 223 (2001) [arXiv:hep-ph/0004270]. F. Krauss, A. Schalicke and G. Soff, *Comput. Phys. Commun.* **174**, 876 (2006) [arXiv:hep-ph/0503087]. G. Gustafson and U. Pettersson, *Nucl. Phys. B* **306**, 746 (1988). L. Lonnblad, *Comput. Phys. Commun.* **71**, 15 (1992). S. Gieseke, P. Stephens and B. Webber, *JHEP* **0312**, 045 (2003) [arXiv:hep-ph/0310083]. S. Gieseke, A. Ribon, M. H. Seymour, P. Stephens and B. Webber, *JHEP* **0402**, 005 (2004) [arXiv:hep-ph/0311208]. S. Gieseke *et al.*, arXiv:hep-ph/0609306. C. W. Bauer and F. J. Tackmann, *Phys. Rev. D* **76**, 114017 (2007) [arXiv:0705.1719 [hep-ph]]. C. W. Bauer, F. J. Tackmann and J. Thaler, arXiv:0801.4028 [hep-ph].
- [24] W. Bartel *et al.* [JADE Collaboration], *Z. Phys. C* **33**, 23 (1986).
- [25] S. Catani, Y. L. Dokshitzer, M. Olsson, G. Turnock and B. R. Webber, *Phys. Lett. B* **269**, 432 (1991).
- [26] S. Bethke, Z. Kunszt, D. E. Soper and W. J. Stirling, *Nucl. Phys. B* **370**, 310 (1992) [Erratum-ibid. B **523**, 681 (1998)].
- [27] S. Catani, Y. L. Dokshitzer, M. H. Seymour and B. R. Webber, *Nucl. Phys. B* **406**, 187 (1993). S. D. Ellis and D. E. Soper, *Phys. Rev. D* **48**, 3160 (1993) [arXiv:hep-ph/9305266].
- [28] Y. L. Dokshitzer, G. D. Leder, S. Moretti and B. R. Webber, *JHEP* **9708**, 001 (1997) [arXiv:hep-ph/9707323]. G. P. Salam and G. Soyez, *JHEP* **0705**, 086 (2007) [arXiv:0704.0292 [hep-ph]].
- [29] J. M. Butterworth, B. E. Cox and J. R. Forshaw, *Phys. Rev. D* **65**, 096014 (2002) [arXiv:hep-ph/0201098]. J. M. Butterworth, A. R. Davison, M. Rubin and G. P. Salam, arXiv:0802.2470 [hep-ph].
- [30] For a recent review of Z' couplings, see P. Langacker, arXiv:0801.1345 [hep-ph].
- [31] G. Hanson *et al.*, *Phys. Rev. Lett.* **35**, 1609 (1975).
- [32] Chris Tully, private communication.
- [33] I. I. Belotelov *et al.*, *Phys. Part. Nucl. Lett.* **4**, 343 (2007).
- [34] L. March, E. Ros and B. Salvachua, ATL-PHYS-PUB-2006-002.
- [35] V. V. Sudakov, *Sov. Phys. JETP* **3** (1956) 65 [*Zh. Eksp. Teor. Fiz.* **30** (1956) 87].
- [36] D. E. Kaplan, K. Rehermann, M. D. Schwartz and B. Tweedie, arXiv:0806.0848 [hep-ph].